

Piotr Śliwiński, Marek St. Węglowski, Janusz Pikuła,
Tomasz Tański, Andrzej N. Wieczorek, Emilia Skołek

Electron Beam Hardening of Nanobainitic Steels

Abstract: Because of the unique combination of their properties, nanobainitic steels containing Si are particularly attractive materials for use in gear manufacturing. However, in order to achieve desired results, it is first necessary to obtain a surface of sufficient hardness (i.e. to increase the hardness of the surface layer using surface hardening techniques). One of such techniques is electron beam hardening. Due to the high power of electron beam welding machines and properties of the electron beam itself, the above-named technology makes it possible to harden workpieces within a wide range of thicknesses. Research-related tests discussed in the article involved the hardening of blocks made of nanobainitic steel (30 mm × 150 mm × 20 mm) using the oscillation-deflected electron beam. Test specimens were subjected to surface hardening with the electron beam using different beam settings. Surface hardening techniques involved both moving the specimen relative to the heat source and quenching only with beam oscillation. As part of the study, finite element simulations were performed along with the validation of results. The test specimens were then subjected to Vickers hardness tests as well as to light microscopic and microstructural tests (using scanning electron microscopy). The test results revealed that the electron beam hardening method made it possible to obtain hardened layers having a thicknesses of up to 1.9 mm. The distribution of hardness in the hardened zone was uniform, whereas the specimens hardened without movement were characterized by a higher average hardness of 674 HV_{0.1}. The average hardness value of the hardened layer amounted to 626 HV_{0.1} in terms of the sample hardened at a speed of 250 mm/min. The results of the FEM numerical calculations were consistent with the results of the actual measurements, indicating that the assumptions and boundary conditions in the FEM modelling of the electron beam quenching process were defined correctly.

Keywords: Electron beam hardening, Gear manufacturing, Sufficient hardness

DOI: 10.17729/ebis.2023.2/3

Introduction

The core of case-hardened low-carbon steel used in the production of toothed wheels is characterised by favourable toughness, whereas the hardened surface is characterised by high hardness and abrasive wear resistance. However, case hardening based on carburising and standard heat treatment does not prevent the cracking of an element

as regards breakage resistance and fatigue strength. In addition, case hardening may intensify crack initiation, primarily affecting internal non-metallic inclusions (oxides and carbides), formed, among others, during the tempering of martensite. The precipitates (as hard and brittle phases) are areas of microcrack formation. Various tests revealed that the refinement of carbides and their uniform distribution in the matrix reduces the

mgr. inż. Piotr Śliwiński, dr inż. Marek St. Węglowski, dr inż. Janusz Pikuła – Sieć Badawcza Łukasiewicz – Górnośląski Instytut Technologiczny (Łukasiewicz Research Network – Upper Silesian Institute of Technology, Centre of Welding)

dr hab. inż. Tomasz Tański – Politechnika Śląska, Wydział Mechaniczny Technologiczny (Silesian University of Technology, Faculty of Mechanical Engineering)

dr hab. inż. Andrzej N. Wieczorek – Politechnika Śląska, Wydział Górnictwa, Inżynierii Bezpieczeństwa i Automatyki Przemysłowej (Silesian University of Technology, Faculty of Mining, Safety Engineering and Industrial Automation)

dr inż. Emilia Skołek – Politechnika Warszawska, Wydział Inżynierii Materiałowej (Silesian University of Technology, Faculty of Materials Engineering)

susceptibility of steel to fatigue cracking. In addition, the presence of retained austenite (in the form of thin layers) in the microstructure significantly restrains crack propagation. Tensile stresses near the top of the crack lead to the transformation of retained austenite into martensite (the so-called TRIP effect), triggering local compressive stresses, which impede further crack propagation. Materials which can help solve the above-presented problems are, e.g. nanobainitic steels, the microstructure of which provides favourable mechanical and functional properties. Nanobainitic steels are characterised by hardness restricted within the range of 600 HV to 700 HV, elongation restricted within the range of 5% to 30% and a tensile strength of 2.5 GPa. In addition, nanobainitic steels containing Si are viewed as a very promising material in the production of toothed wheels. Steels containing silicon are characterised by potential making it possible to prevent the precipitation of carbides (responsible for the brittleness of steel) and by very attractively combined mechanical and functional properties [1–8]. In order to further improve their abrasive wear resistance (or when preparing the deposition of hard protective layers), toothed wheels made of nanobainitic steel can also be subjected to case hardening. One of the methods perfectly suitable for this process is electron beam hardening. The aforesaid method enables the hardening of elements characterised by complex geometry as well as allows the making of hardened layers within a very wide thickness range (from several micrometres to several millimetres). In addition, the method enables the hardening of individual surface fragments or, owing to the possibility of dynamic beam deflection, the hardening of workpieces without moving them. The performance of the case hardening process under vacuum conditions makes hardened surfaces protected against oxidation [9–11].

Overview of reference publications

The electron beam hardening method is used in industry, with numerous publications presenting results of tests aimed to optimise the process. One of such works is publication [12], which discusses results concerning the attempted optimisation of the electron beam hardening process. The tests discussed in the aforesaid study involved the use of steel containing C (0.42%), Mn (0.6%), Cr (0.96%) and Si (0.37%). The effect of the specimen

travel rate and electron beam power on heating and cooling rates was determined using a mathematical model. The test revealed that the heating rate grew along with increasing specimen travel rates without changing electron beam power (Fig. 1). A further increase in the specimen travel rate only slightly affected the heating rate, which neared the limit value in relation to rates exceeding 1800 mm/min.

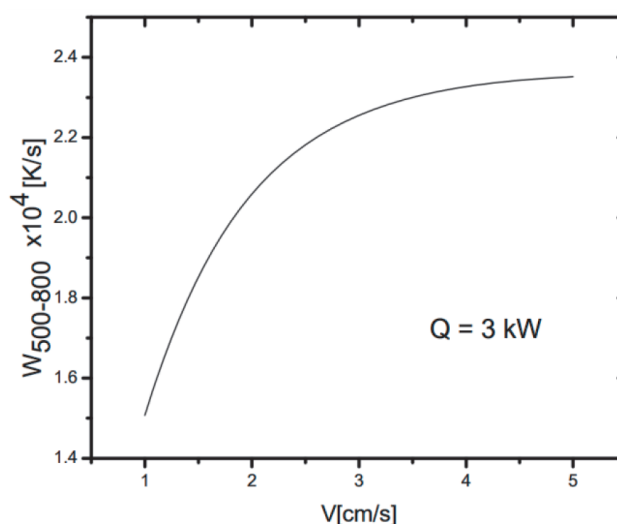


Fig. 1. Effect of the specimen travel rate on the heating rate [12]

The authors of the publication observed that an increase in electron beam power was accompanied by the linearly increasing heating rate (combined with the constant specimen travel rate). The calculations also revealed that the cooling rate was significantly affected by the specimen travel rate (Fig. 2) and was only slightly influenced by electron beam power. The analysis of the numerical test

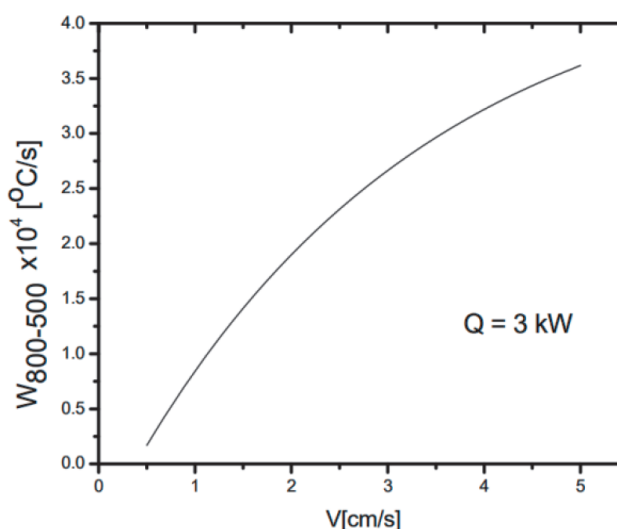


Fig. 2. Effect of the specimen travel rate on the resultant cooling rate [12]

results led to the conclusion that the heating and cooling rates as well as the general effectiveness of the electron beam hardening process depended primarily on the velocity of specimen displacement in relation to the heat source.

Article [13] presents results of mathematical simulations concerning the effect of electron beam hardening process parameters on the microstructure and the depth of hardened layers. The simulation was followed by tests involving actual elements (made of steel grade 55). Changes included those of oscillation frequency, accelerating voltage and electron beam current. The hardened layers were characterised by a surface hardness of up to 60 HRC and the depth restricted within the range of 0.3 mm to 1.1 mm. The results of mathematical simulation and those of actual tests concerning parameters subjected to analysis (the tests did not include the specimen travel rate) revealed that the resultant electron beam power had the most significant effect on the cooling rate and, consequently, on surface hardness. In turn, the density of electron beam energy on the workpiece surface was decisive for the depth of specimens hardening.

One of the entities applying the electron beam hardening process in industrial practice is the Production Engineering Department of the Isuzu Motors Ltd., which performed tests concerning the use of the electron beam hardening technology in the automotive industry [14]. The tests revealed the high effectiveness of the method and enabled its application in the automotive sector. The test material was steel grade 34CrMo4. The material was heated locally by the oscillating electron beam. The test aimed to verify the influence of beam effect time-related changes. The maximum obtainable hardened depth (without the appearance of the liquid phase) amounted to 0.9 mm. The favourable test results encouraged the authors to perform the electron beam hardening of Isuzu B6 engine tappets and of the gearbox synchroniser clamping ring. Figure 1 presents the distribution of hardness in the electron beam-hardened tappet of the Isuzu B6 engine.

Publication [15] discusses tests concerning various beam deflection patterns on properties of

electron beam hardened layers. The test material was steel containing C (0.41%), Si (0.25%), Mn (0.69%), Cr (1.04%) and Mo (0.20%). The tests results revealed that the shape of oscillation could affect numerous properties of the surface layer (the greatest effect being on the shape of the cross-section of the hardened layer) (Fig. 3). In accordance with the test results, deflection patterns containing the field additionally deflected in the direction parallel to the direction of displacement (and not only the line deflected in the perpendicular direction) improved the depth of hardening in relation to the same specimen travel rate (Fig. 3). The test revealed that the shape of an oscillation pattern did not affect the value of surface hardness obtained in the process.

Results concerning the hardening of steel 40CrMn involving the use of the oscillating electron beam are presented in publication [16]. The hardening procedure involved the making of three parallel beams with varying values of overlaps between the beads. In relation to a base material hardness of 300 HV, the surface treatment led to an increase in hardness to approximately 650 HV. At the same time, it was possible to observe the unfavourable effect of multi-run hardening, triggered by the mutual tempering of successive beads. The tempering phenomenon was attributed to interaction between thermal cycles of successive runs, which decreased the hardness in the tempered layer to approximately 400 HV.

Article [17] presents test results concerning the effect of the electron beam hardening of tool steel AISI D3, the hardness of which amounted to approximately 650 HV0.1. Parameters changed during the process included a specimen travel rate of 0.6 m/min, 1.2 m/min and 1.8 m/min. The specimen which had been hardened using the highest rate contained the surface layer characterised by the highest hardness (amounting to approximately 1400 HV0.1). In each specimen it was possible to observe the presence of the interlayer characterised by hardness reduced to approximately 400 HV0.1. The distribution of hardness in all the specimens is presented in Figure 2.

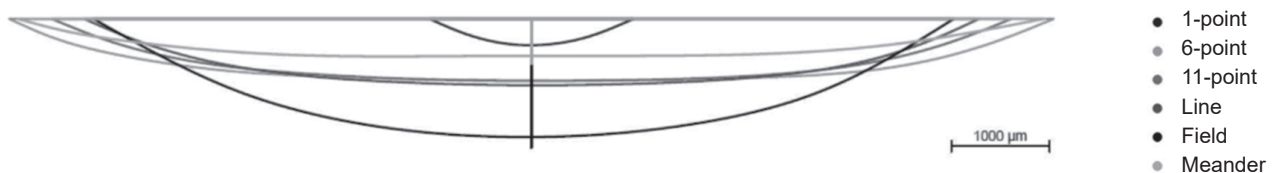


Fig. 3. Effect of the deflection mode and electron beam focusing current on the geometry of hardened layers [15]

As can be seen on the basis of the above-presented reference publications, electron beam hardening enables the obtainment of layers hardened within a wide range of thicknesses and of various geometry (in terms of numerous steel grades). The key aspect of the electron beam hardening process is the appropriate adjustment of parameters including beam power, the location of the beam focus in relation to the surface of the material subjected to hardening, the rate of beam movement in relation to the heat source as well as the shape and frequency of oscillation. The study discussed further in the article aimed to investigate the electron beam hardening of nanobainitic steel and the development of a validated FEM model.

Tests and results

A research programme included the development of an FEM model, the making of validation hardened specimens, and the performance of hardness measurements as well as microstructural analysis based on light and scanning electron microscopy (SEM).

The material subjected to treatment was steel, the chemical composition of which is presented in Table 1. The chemical composition analysis was performed using a Magellan Q8 Optical spark emission spectrometer (Bruker Elemental GmbH).

Table 1. Chemical composition of the test nanobainitic steel

C, %	Mn, %	Si, %	Cr, %	Ni, %	Cu, %
0.386	0.835	1.129	1.128	0.077	0.169
Mo, %	Ti, %	V, %	W, %	P, %	S, %
0.031	0.0053	0.0094	0.012	0.0046	0.0007

The nanobainitic microstructure in the test material was obtained using heat treatment. Because of the application of a heat treatment procedure developed at the Faculty of Materials Engineering of the Warsaw University of Technology (patent number: PAT.234490 [18]), it was possible to significantly reduce the time needed to obtain the carbon-free nanobainitic structure. In addition to enabling the reduction of process time, the heat treatment procedure made it possible to introduce a small amount of submicron martensite, which substantially improved the hardness and wear resistance of the steel.

Heat treated rollers having a diameter of 170 mm were used to make disks having a thickness of 20 mm. Afterwards, the plates were cut to obtain

30 mm wide strips. The obtained material blocks were 150 mm long, 30 mm wide and 20 mm thick. The area subjected to hardening had dimensions of 150 mm × 30 mm.

Case hardening tests were performed at the Welding Centre of the Łukasiewicz Research Network – Upper Silesian Institute of Technology, using an XW150:30 electron beam welding machine (Cambridge Vacuum Engineering). The test specimens were fixed to an aluminium block having dimensions 300 mm × 200 mm × 30 mm (in order to improve the discharge of heat from the surface subjected to hardening, because of the overly low thermal capacity of single test specimens). Due to the tempering of the hardened layer (observed during the multi-run electron beam hardening process), the authors decided that the entire surface area should be subjected to hardening performed in one run [16]. The test specimens were hardened using two different hardening techniques.

The first method consisted in the simultaneous hardening of the entire surface area of the specimen using a dedicated pattern of oscillation adjusted to the shape of the specimen surface area (i.e. a rectangle having dimensions of 150 mm × 30 mm). The only variable during the process was the heating rate; the specimen was not moved during the process.

The second method involved the displacement of the specimen in relation to the heat source and the application of the electron beam oscillating at a frequency of 200 Hz in the field having dimensions of 30 mm × 6 mm. In the above-named case, there were two process variables, i.e. beam power and the specimen travel rate.

Regardless of the hardening technique, the specimens were hardened using an accelerating voltage of 140 kV. The working distance amounted to 420 mm, whereas the pressure in the working chamber amounted to $1 \cdot 10^{-4}$ mbar. The electron beam was defocused. The current of the focusing lens amounted to 610 mA, i.e. by 100 mA less than that in the beam focused on the point at a distance of 420 mm.

The optimisation of the hardening process necessitated the development of an FEM model of elements (to be hardened), which was subjected to validation based on two special specimens with incised grooves of variable depth. The thickness of the material above the grooves (where thermocouples were fixed) amounted to 2.0 mm, 3.4 mm, 5.0 mm, 6.5 mm and 8.0 mm) (Fig. 4).

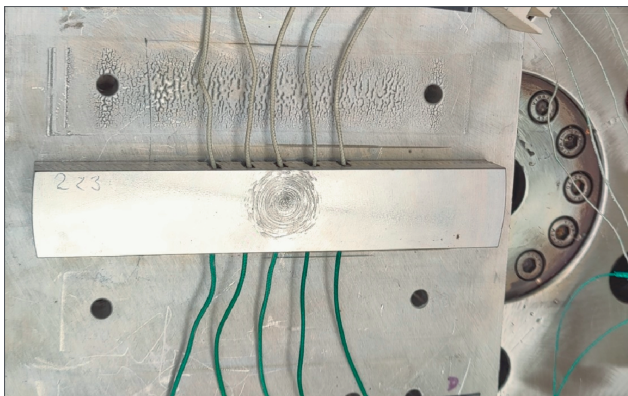


Fig. 4. Validation specimen (with thermocouples) fixed to the aluminium block (300 mm × 200 mm × 30 mm)

The specimens were hardened using the following parameters:

- 3.5 seconds of heating affecting the specimen which was not moved in relation to the heat source,
- specimen travel rate of 250 mm/min and an electron beam current of 25 mA in relation to the specimen which was moved in relation to the heat source.

Afterwards, the specimens were subjected to metallographic tests (performed using a light microscope and a scanning electron microscope (SEM)) and hardness measurements.

The tests involved the use of the finite element method (FEM). The FEM-based numerical models were developed on the basis of the actual geometry of the elements subjected to hardening (Fig. 4). The geometry (Fig. 5) included the element subjected to hardening (also the milled notches used in temperature measurements) and the aluminium base on which the element was placed. The geometry of the thermocouples was taken into consideration as the former constituted an additional element discharging heat. The initial modelling tests revealed that taking the above-named geometry into consideration significantly affected the value of temperature in the area (particularly at points T1, T2 and T3, where the distance between the surface subjected to hardening and the temperature measurement point was the shortest). The mesh of finite elements (Fig. 6), based on the previously prepared geometry, was characterised by the highest density (the maximum size of the elements amounting to 0.2 mm) in the areas directly affected by the electron beam and subjected to temperature measurements. The finite elements were ascribed thermal material properties of the test steel and the chemical composition consistent with information presented in Table 1.

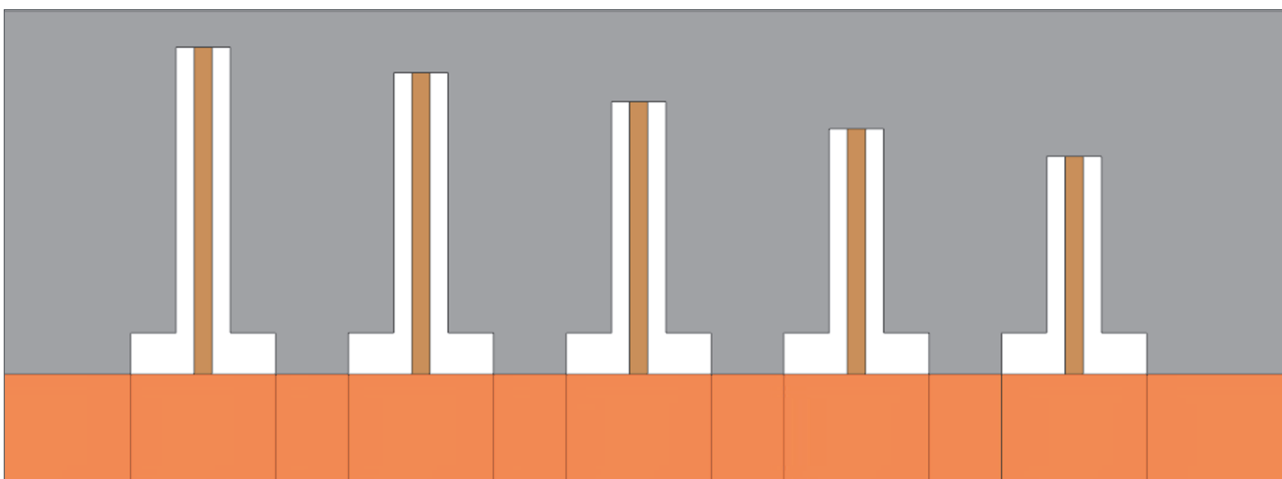


Fig. 5. Fragment of the geometry used to prepare the mesh of finite elements (grey colour – element subjected to hardening, brown colour – thermocouples and the orange colour – base where the element subjected to hardening was placed)

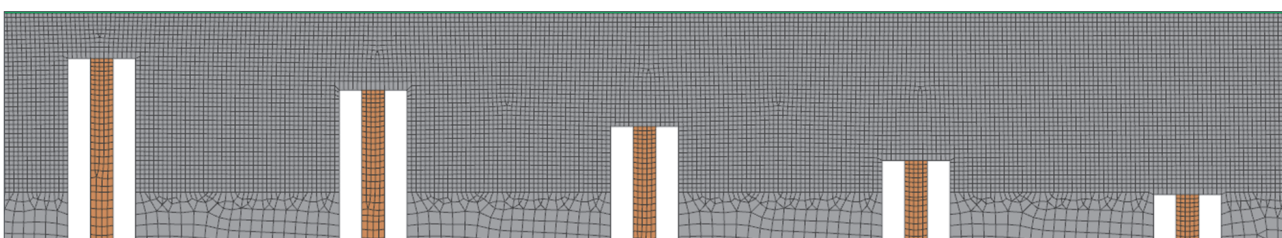


Fig. 6. Fragment (temperature measurement area) of the mesh of finite elements used in the modelling of the electron beam hardening process

The FEM model included the exchange of heat with the environment through thermal radiation; the phenomenon of convection was not taken into consideration as the process was performed in vacuum. The amount of heat radiated by the body was implemented using the Stefan-Boltzmann law (1), taking into account surface emissivity factor ε and the difference of body temperature T and that of environment (surrounding the body) T_0 .

$$q_s = \varepsilon\sigma(T^4 - T_0^4) \quad (1)$$

where

σ – Stefan-Boltzmann constant, $5.67 \cdot 10^{-8} \text{ kg/s}^3\text{K}^4$

Equation (1) was transformed in calculations in order to identify heat exchange coefficient α_s , resulting from the heat radiation phenomenon (2) [19, 20].

$$\alpha = \varepsilon\sigma(T + T_0) (T^2 + T_0^2) \quad (2)$$

The emissivity factor adopted in the model amounted to 0.8. The flow of heat was defined using the Fourier law of heat conduction, i.e. the primary law concerning quantitative conduction (3). The unsteady flow of heat in the isotropic medium, in the presence of internal volumetric heat sources, was also described using the Fourier equation (4).

$$q = -\lambda(T)\text{grad}T \quad (3)$$

$$c(T)\rho(T)\frac{\partial T}{\partial t} - \text{div}[\lambda(T)\text{grad}T] - Q = 0 \quad (4)$$

Because of the fact that the electron beam hardening process is a complex phenomenon, industrial

practice involves the use of a simplified volumetric heat source in the form of a cylinder or a truncated cone and based on Gaussian distribution. The hardening process subjected to analysis was characterised by high electron beam displacement rates, amounting to a maximum of 150,000 mm/s. Because of the foregoing, in the models, the electron beam effect was modelled as the heat source in the form of a cylinder having dimensions consistent with the oscillation width of the actual hardening process and the electron beam diameter. The amount of energy was identified on the basis of the actual hardening process.

Analysis of test results

In order to prepare the appropriate observation area, the specimens were cut along the longer side and, afterwards, subjected to grinding, polishing and etching in 3% Nital. Next, the specimens were observed using an Eclipse MA200 light microscope (Nikon). The temperature measurement results and the cross-section of the specimen subjected to hardening (without displacement) for a time of 3.5 seconds are presented in Figures 7 and 8. Figure 9 presents the field of maximum temperature identified during the hardening process (calculated using the FEM). The diagram presented in Figure 7 reveals that both at the point having a thickness of 2 mm and at a point having a thickness of 3.4 mm, the temperature of the material reached 727°C. The foregoing enabled the austenitic transformation followed by the transformation of austenite into martensite (as a result of

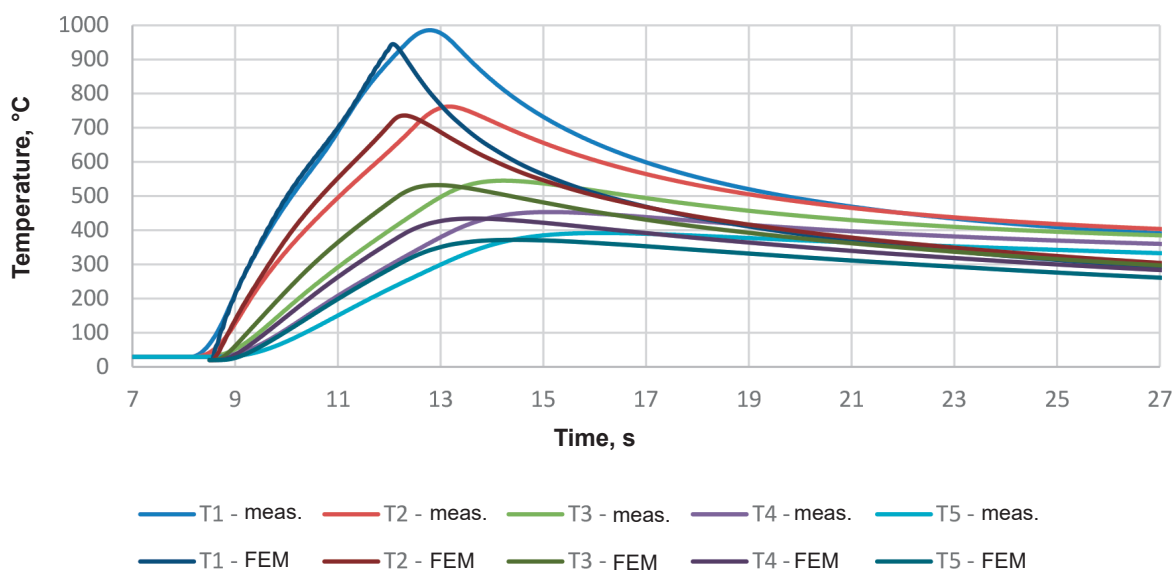


Fig. 7. Diagram of changes of temperature in time (calculated using FEM) and in relation to each thermocouple fixed on the motionless specimen hardened for 3.5 s; T1 – thermocouple fixed at the point of the material having a thickness of 2.0 mm, T2 – 3.4 mm, T3 – 5.0 mm, T4 – 6.5 mm and T5 – 8.0 mm

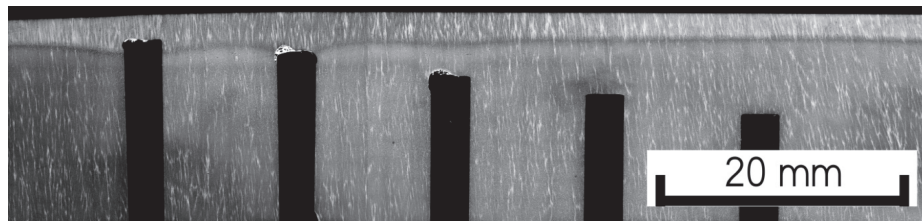


Fig. 8. Longitudinal section of the specimen subjected to hardening for 3.5 sec, without being moved in relation to the heat source

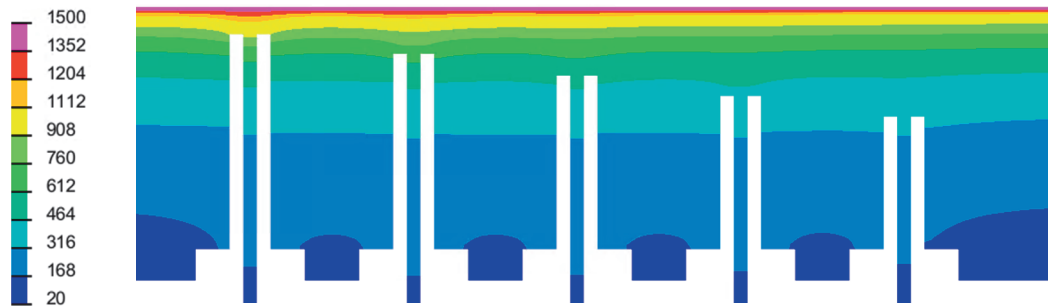


Fig. 9. Field of the maximum temperature of the longitudinal section of the specimen subjected to hardening for 3.5 sec, without being moved in relation to the heat source

sufficiently fast cooling). The temperature measurement results corresponded to the macrostructure presented in Figure 8, where in the material (both above the first and the second groove, on the left) it was possible to observe a structure changed in relation to the base material.

Figures 10 and 11 present the results of calculations and temperature measurements as well as a photograph of the longitudinal section of the specimen hardened (and moving in relation to the

heat source) at a travel rate of 250 mm/min and using an electron beam current of 25 mA. Figure 12 presents the field of maximum temperature (calculated using the finite element method), determined during the hardening process. As regards the above-named specimen, only in relation to the material having a thickness of 2 mm it was possible to observe temperature exceeding 727°C. As a result, only at the aforesaid point, the material was hardened right through, which was reflected

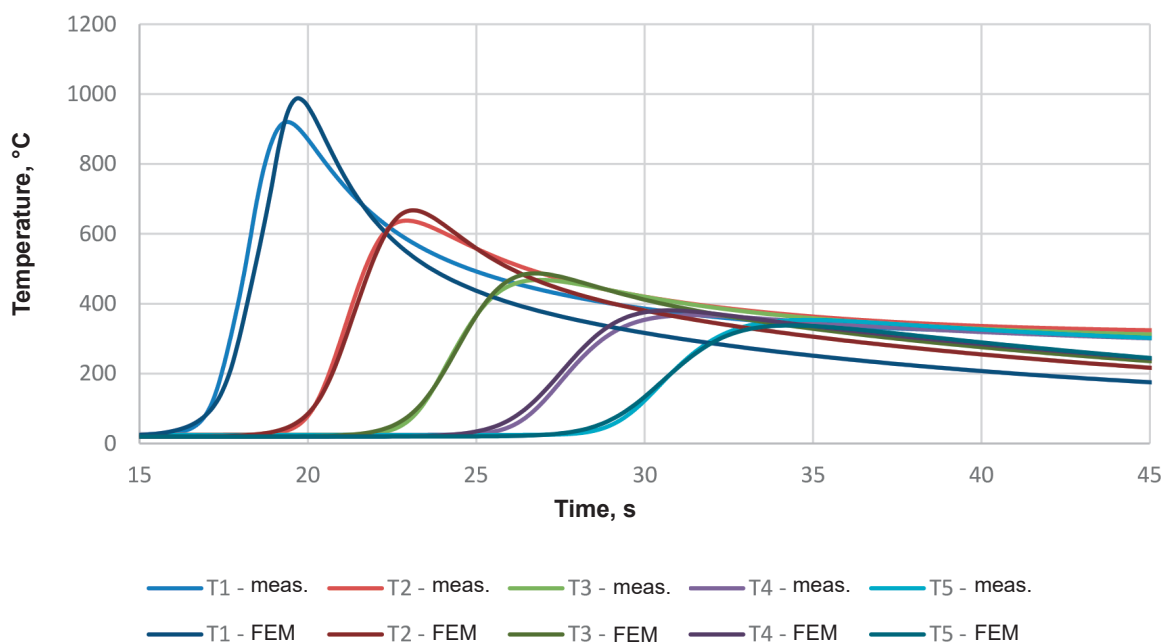


Fig. 10. Diagram of changes of temperature in time (calculated using FEM) and in relation to each thermocouple fixed on the moving specimen hardened for 3.5 s, using a specimen travel rate of 250 mm/min and an electron beam current of 25mA; T1 – thermocouple fixed at the point of the material having a thickness of 2.0 mm, T2 – 3.4 mm, T3 – 5.0 mm, T4 – 6.5 mm and T5 – 8.0 mm

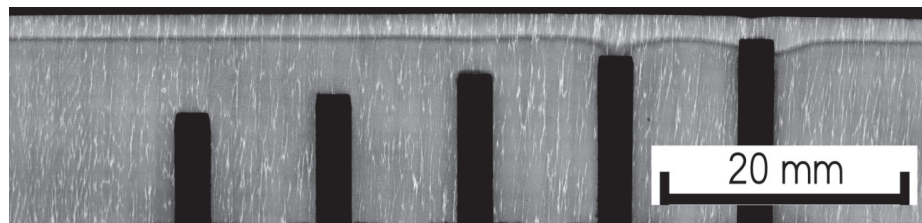


Fig. 11. Longitudinal section of the specimen moving in relation to the heat source at a travel rate of 250 mm/min and hardened using an electron beam current of 25 mA

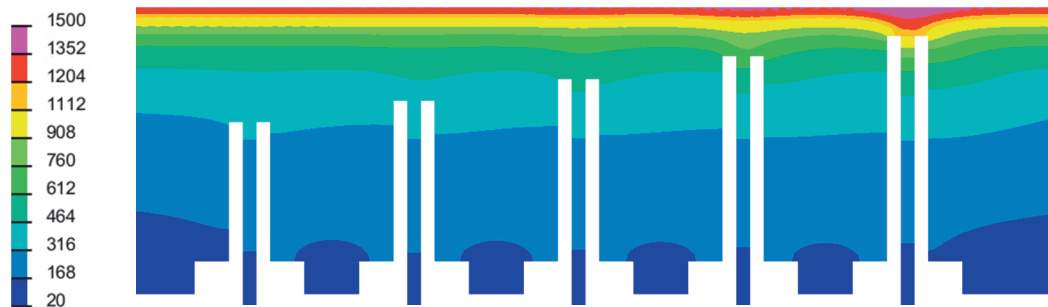


Fig. 12. Field of the maximum temperature of the longitudinal section of the specimen moving in relation to the heat source at a travel rate of 250 mm/min and hardened using an electron beam current of 25 mA, °C

in the macrostructure of the hardened layer presented in Figure 8.

Figure 13 presents the microstructure of the base material of nanobainitic steel having the chemical composition presented in Table 1. Figure 14 presents the comparison of the microstructure of the surface layer of both specimens. Figure 15 presents the comparison of the microstructure of the interlayer of both specimens.

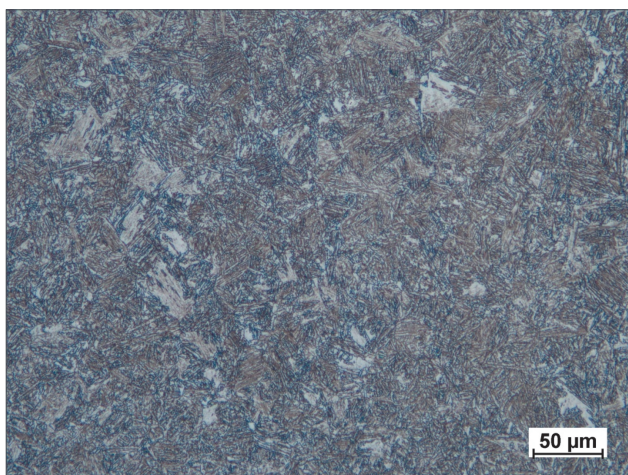


Fig. 13. Microstructure of nanobainitic steel 35HGS

Hardness measurements under a load of HV0.1 were performed using an automatic hardness tester (KB Prüftechnik). The measurements were performed every 50 μm – to the material border or to a depth of 4 mm. Each specimen had five measurement lines. Each measurement line, drawn over a successive groove milled in the specimen, consisted

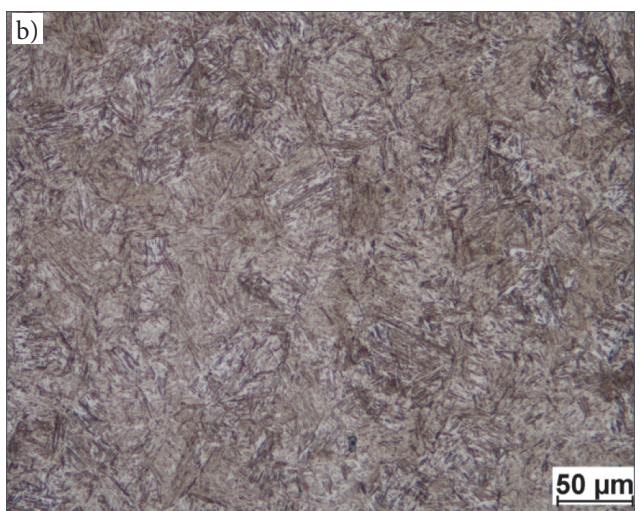
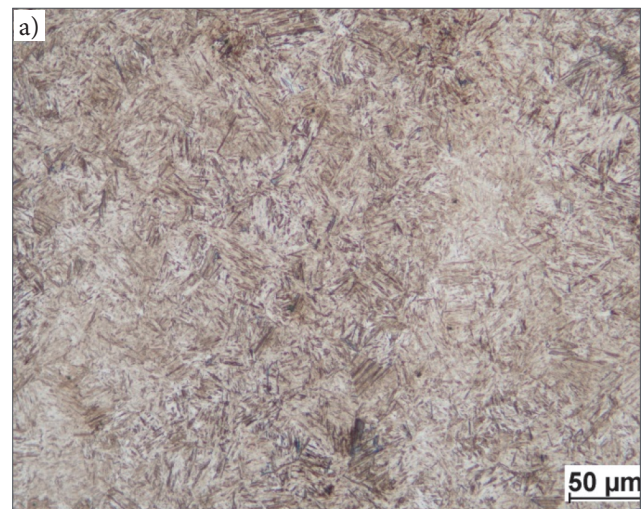


Fig. 14. Microstructure of the surface (hardened) layer: a) specimen subjected to hardening for 3.5 s, not moved in relation to the heat source and b) specimen subjected to hardening, using a specimen travel rate of 250 mm/min and an electron beam current of 25 mA

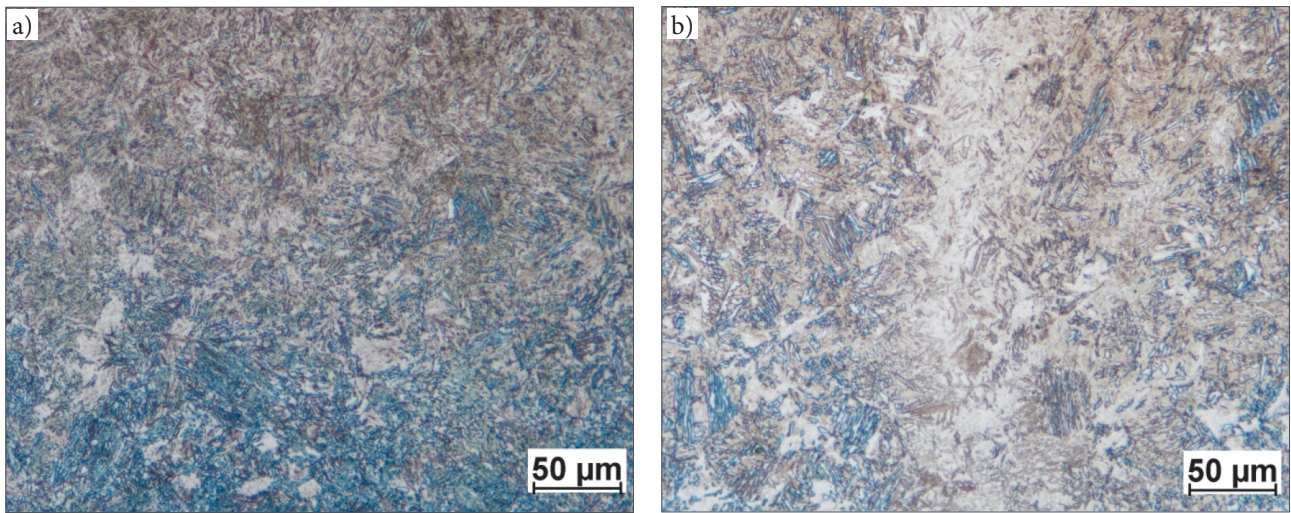


Fig. 15. Microstructure of the interlayer: a) specimen subjected to hardening for 3.5 s, not moved in relation to the heat source and b) specimen subjected to hardening, using a specimen travel rate of 250 mm/min and an electron beam current of 25 mA

of between 35 and 80 points. The measurements were performed on the cross-sections of the specimens. Figures 16 and 17 present the distributions

of hardness in relation to all the measurement lines of both specimens. The measurement results corresponded with metallographic observations.

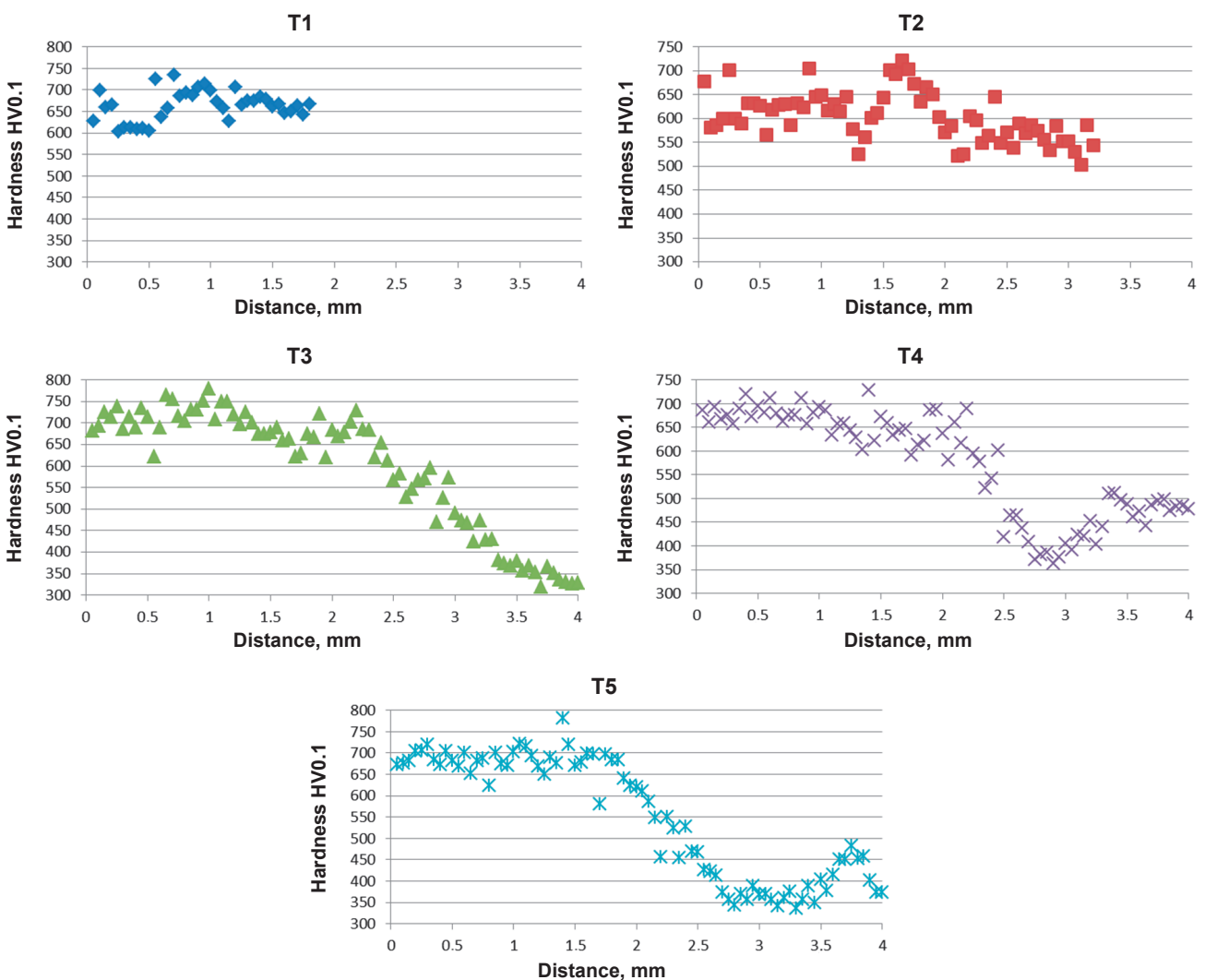


Fig. 16. Hardness distribution in relation to all the measurement lines of the specimen subjected to hardening for 3.5 s, without being moved in relation to the heat source: a) T1 – measurement at the point where the material had a thickness of 2.0 mm, b) T2 – 3.4 mm, c) T3 – 5.0 mm, d) T4 – 6.5 mm and e) T5 – 8.0 mm

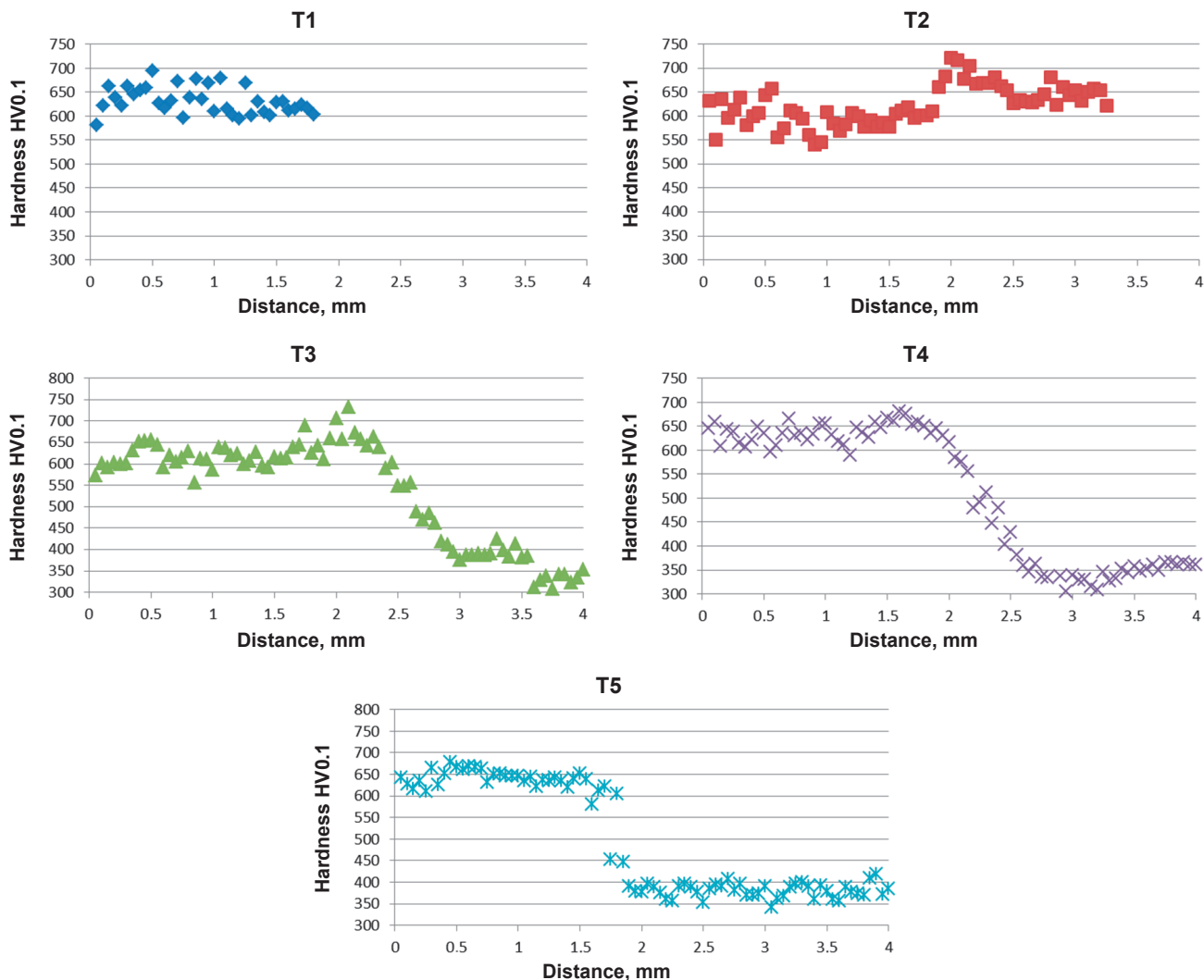


Fig. 17. Hardness distribution in relation to all the measurement lines of the specimen subjected to hardening performed using a specimen travel rate of 250 mm/min and an electron beam current of 25 mA: a) T1 – measurement at the point where the material had a thickness of 2.0 mm, b) T2 – 3.4 mm, c) T3 – 5.0 mm, d) T4 – 6.5 mm and e) T5 – 8.0 mm

In the specimen which was not moved in relation to the heat source, the average hardness of the hardened layer amounted to 674 HV0.1. In turn, in the specimen hardened at a specimen travel rate of 250 mm/min, the average hardness of the hardened layer amounted to 626 HV0.1. In the zone of the greatest material thickness (T5), the thickness of the hardened layer in the specimen not moved in relation to the heat source amounted to approximately 1.9 mm. Below the above-named layer it was possible to observe a zone characterised by a decrease in hardness. In the specimen hardened at a specimen travel rate of 250 mm/min, the thickness of the hardened layer in zone T5 was restricted within the range of approximately 1.7 mm to 1.8 mm.

The FEM model and identified thermal cycles were used to calculate hardness fields presented in Figures 18 and 19. The values calculated in the area

of point T5 in the line perpendicular to the hardened surface are presented in Figures 20 and 21.

In the model of the specimen subjected to hardening for 3.5 s and not moved in relation to the heat source, the maximum hardness value (in the area subjected to analysis) amounted to 630 HV. The thickness of the hardened layer amounted to approximately 1.6 mm.

In the model of the specimen subjected to hardening performed using a specimen travel rate of 250 mm/min and an electron beam current of 25 mA, the maximum hardness value (in the area subjected to analysis) amounted to 589 HV. The thickness of the hardened layer amounted to approximately 1.6 mm.

The FEM-based analysis revealed that the use of the hardening method involving the displacement of the specimen at a rate of 250 mm/min and the application of an electron beam current of 25 mA

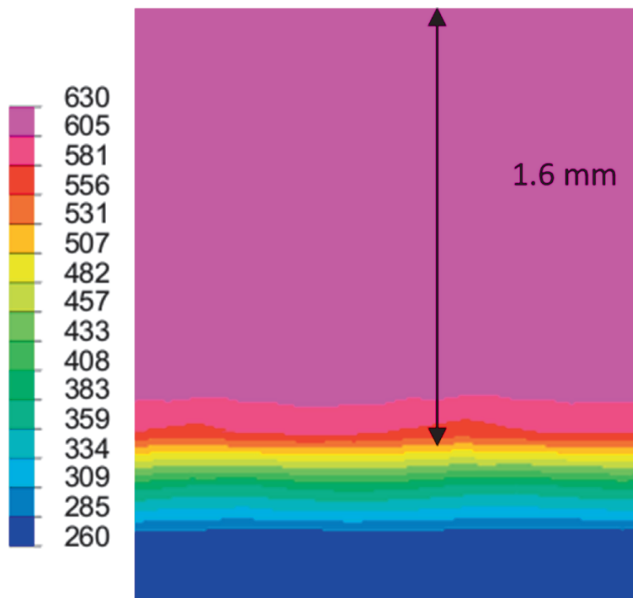


Fig. 18. Field of hardness identified in the area outside the grooves of the specimen subjected to hardening for 3.5 s, without being moved in relation to the heat source

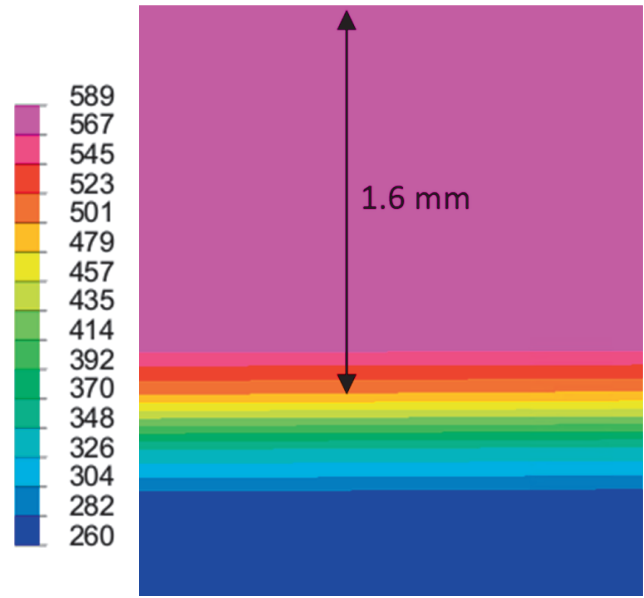


Fig. 19. Field of hardness identified in the area outside the grooves of the specimen subjected to hardening performed using a specimen travel rate of 250 mm/min and an electron beam current of 25 mA

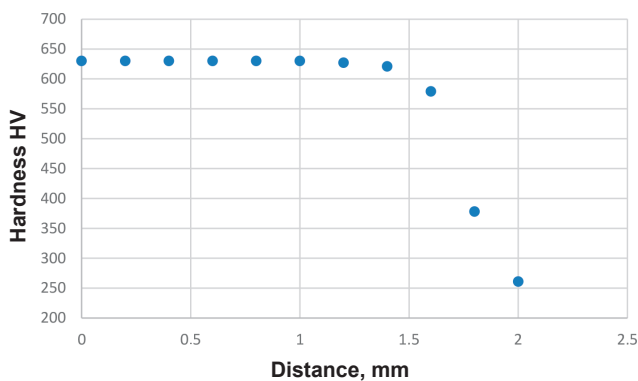


Fig. 20. Distribution of hardness in the area outside the grooves of the specimen subjected to hardening for 3.5 s, without being moved in relation to the heat source

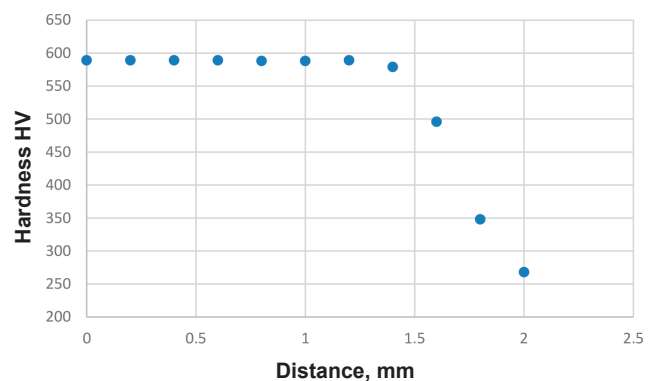


Fig. 21. Distribution of hardness in the area outside the grooves of the specimen subjected to hardening performed using a specimen travel rate of 250 mm/min and an electron beam current of 25 mA

enabled the obtainment of hardened depth similar to that obtained using the method where the specimen was hardened for 3.5 s, without being moved in relation to the heat source. However, the hardening method not involving the displacement of the specimen made it possible to obtain higher hardness (by approximately 7%).

The specimens were also subjected to observations involving the use of an S5500 scanning electron microscope (Hitachi). The specimens were sampled from the core, subsurface zone, decreased hardness zone and the zone of the lowest hardness. Figure 22 presents the microstructure of the base material. Figure 23 presents the comparison of the microstructure of the surface layer of both specimens. Figures 24 and 25 present the comparison

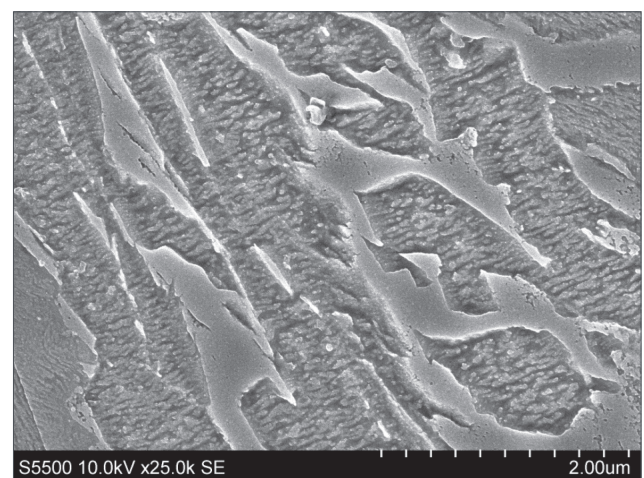


Fig. 22. Microstructure of the base material

of the microstructure of the interlayer (characterised by lower hardness and located between

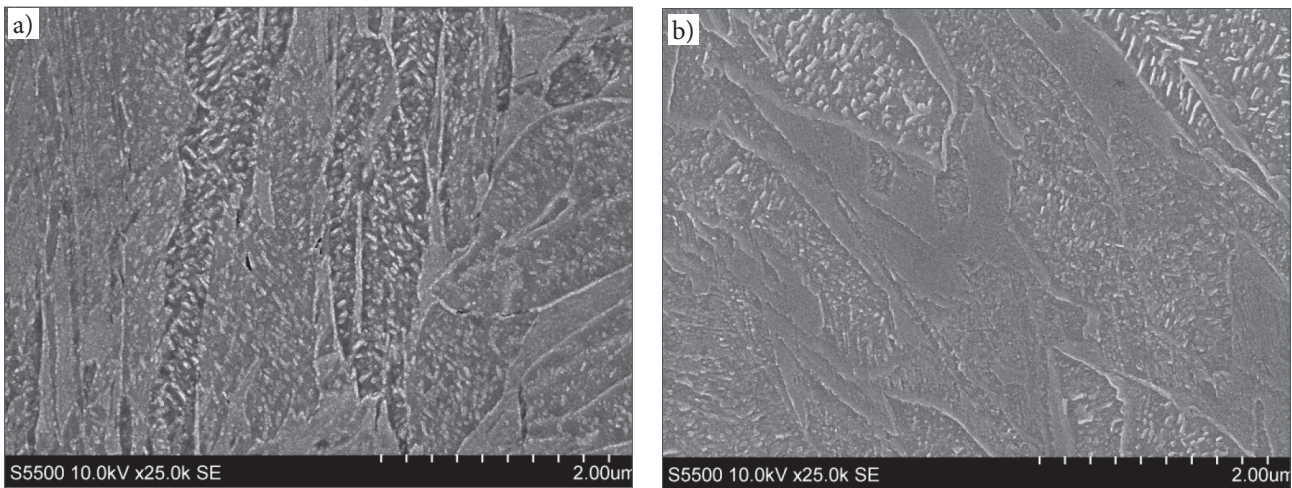


Fig. 23. Microstructure of the surface layer: a) specimen subjected to hardening performed using a specimen travel rate of 250 mm/min and an electron beam current of 25 mA and b) specimen subjected to hardening for 3.5 s, without being moved in relation to the heat source

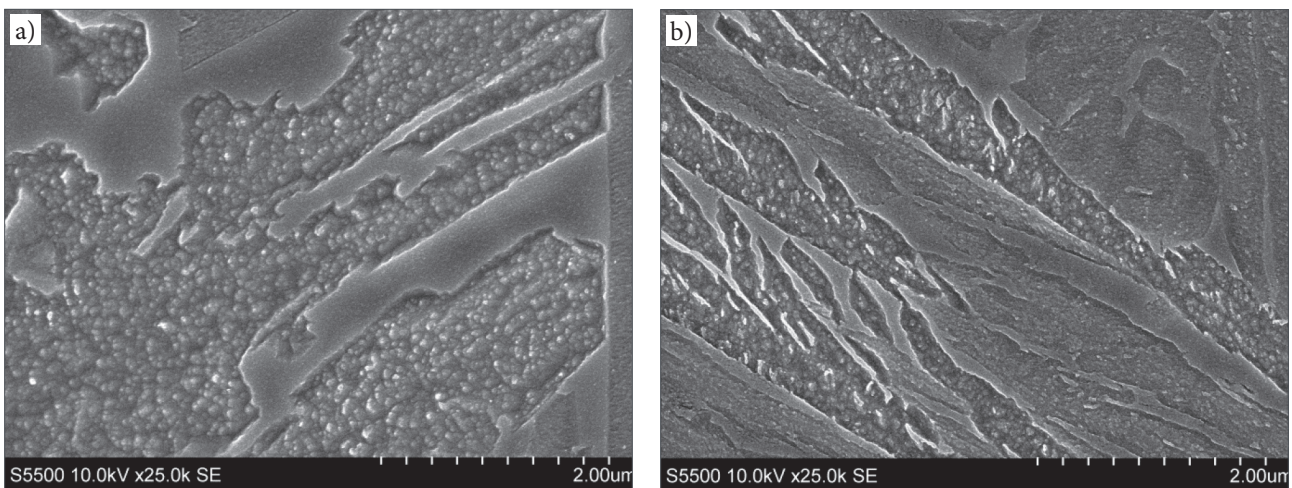


Fig. 24. Microstructure of the layer characterised by reduced hardness (located approximately 1.6 mm under the hardened surface): a) specimen subjected to hardening performed using a specimen travel rate of 250 mm/min and an electron beam current of 25 mA and b) specimen subjected to hardening for 3.5 s, without being moved in relation to the heat source

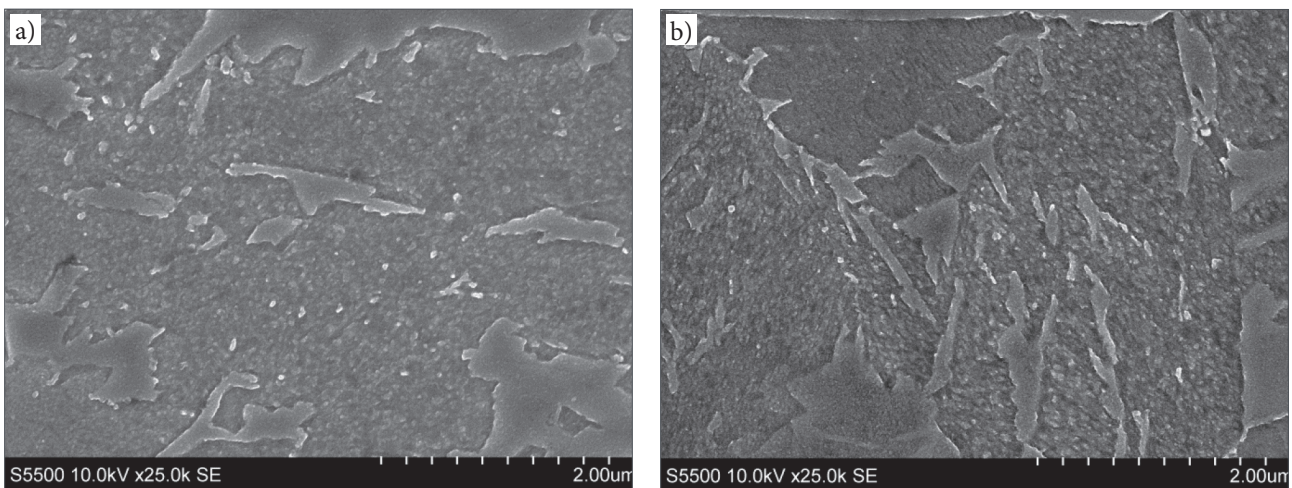


Fig. 25. Microstructure of the layer characterised by reduced hardness (located approximately 2.5 mm under the hardened surface): a) specimen subjected to hardening performed using a specimen travel rate of 250 mm/min and an electron beam current of 25 mA and b) specimen subjected to hardening for 3.5 s, without being moved in relation to the heat source

approximately 1.6 mm and approximately 2.5 mm under the hardened surface) of both specimens.

The near-weld zone contained tempered martensite. The tempering process could be attributed to the relatively slow specimen travel rate, which translated into the long heat effect. Deeper, in the area characterised by a gradual decrease in hardness, it was possible to observe the mixture of the ferritic, martensitic and austenitic microstructures. In some areas it was also possible to notice fine carbide precipitates within grains and along grain boundaries. Although the microstructure became more comparable with the ferritic-austenitic microstructure of the core, the areas characterised by the lowest hardness contained some martensitic zones. Fine-dispersive carbides precipitated both in ferrite and martensite, which led to a decrease in hardness (in comparison with that of the core). The core of the specimen contained the typical sub-micron ferritic-austenitic microstructure with either the small number or the lack of carbides.

Conclusions

The research work discussed in the article involved the hardening of nanobainitic steel using the oscillating electron beam. The obtained test results justified the formulation of the following conclusions:

- electron beam hardening method made it possible to obtain hardened layers having a depth of up to 1.9 mm and, at the same time, protected against oxidation;
- transition line between the base material and the hardened layer was parallel outside areas characterised by the significant reduction of material thickness, where the thickness of the hardened layer was greater;
- hardness distribution in the hardened zone was uniform. In both specimens it was possible to observe a zone of reduced hardness, located under the hardened layer. The thickness of the hardened layer in both specimens was similar and amounted to 1.9 mm (in the specimen hardened without displacement) and to 1.75 mm (in the specimen subjected to hardening performed using a specimen travel rate of 250 mm/min);
- specimens subjected to hardening without displacement were characterised by the higher average hardness of the hardened layer. The average hardness of the layer subjected to hardening without displacing the specimen in relation to the heat source amounted to 674 HV0.1. In turn,

the average hardness of the specimen subjected to hardening performed using a specimen travel rate of 250 mm/min amounted to 626 HV0.1;

- FEM-based calculations results were consistent with actual measurement results, which indicated the proper definition of assumptions and boundary conditions in the FEM-based modelling of the electron beam hardening process;
- analysis revealed that both electron beam hardening methods enabled the obtainment of a similar hardened depth. However, the method where the specimen was not moved in relation to the heat source enabled the obtainment of hardness which was by approximately 7% higher than that obtained using the method involving the displacement of the specimen.

Acknowledgements

The research-related tests were performed within the project *The Development of Innovative Hybrid Surface Layers Composed of Wear-Resistant Coatings for Teeth of Toothed Gears in Drive Units of Conveyors Operated under Harsh Service Conditions*; contract no.: TECHMATSTRATEG-III/0028/2019-00, financed by the National Centre for Research and Development RP.

References

- [1] Ríos-Diez O., Aristizábal-Sierra R., Serna-Giraldo C., Eres-Castellanos A., García-Mateo C.: Wear behavior of nanostructured carbo-austempered cast steels under rolling-sliding conditions. *Journal of Materials Research and Technology*, 2021, no. 11, 1343. DOI: 10.1016/j.jmrt.2021.01.094.
- [2] Leiro A., Vuorinen E., Sundin K.G., Prakash B., Sourmail T., Smanio V., Caballero F.G., Garcia-Mateo C., Roberto E.: Wear of nano-structured carbide-free bainitic steels under dry rolling-sliding conditions. *Wear*, 2013, vol. 298–299, pp. 42–47. DOI: 10.1016/j.wear.2012.11.064.
- [3] Solano-Alvarez W., Pickering E.J., Bhadeshia H.K.D.H.: Degradation of nanostructured bainitic steel under rolling contact fatigue. *Materials Science and Engineering: A* 2014, vol. 617, 156. DOI: 10.1016/j.msea.2014.08.071.
- [4] Popelyukh A.I., Veselov S.V., Munkueva D.D.: Properties of Steel with Nanobainitic Structure. *Metal Science and Heat Treatment*, 2022, vol. 63, no. 4, 655. DOI: 10.1007/s11041-022-00751-8.
- [5] Yurchenko A.N., Simonova Y.N.: Microstructural features, mechanical properties and heat treatment of bainitic steels. *Vest. Permsk. Nats. Issled. Politekh. Univ*, 2015, vol. 18, no. 3, pp. 160.
- [6] Sidhu G., Bhole S.D., Essadiqi E. et al.: Characterization of Isothermally Heat-Treated High Carbon Nanobainitic Steels. *Journal of Materials Engineering and*

- Performance, 2013, vol. 22, no. 10, 3070. DOI: 10.1007/s11665-013-0581-4.
- [7] Ríos-Diez O., Aristizábal-Sierra R., Serna-Giraldo C., Jimenez J.A., Garcia-Mateo C.: Development of Nano-bainitic Microstructures in Carbo-Austempered Cast Steels: Heat Treatment, Microstructure and Properties. *Metals*, 2020, vol. 10, no. 5, 635. DOI: 10.3390/met10050635.
- [8] Sourmail T., Smanio V., Ziegel C. et al.: Novel Nanostructured Bainitic Steel Grades to Answer the Need for High-Performance Steel Components (NANOBAIN). European Commission, Directorate-General for Research and Innovation 2013. DOI: 10.2777/958.
- [9] Śliwiński P., Węglowski M.S., Kwieciński K., Wiczorek A.: Electron beam surface hardening – an overview. *Institute of Welding Bulletin*, 2022, no. 1, pp. 9. DOI: 10.17729/ebis.2022.1/1.
- [10] Pilarczyk J., Węglowski M.S.: Coating generation and surface modification using electron beam in welding engineering. *Welding Technology Review*, 2015, vol. 87. DOI: 10.26628/ps.v87i9.449.
- [11] Valkov S., Ormanova M., Petrov P.: Electron-Beam Surface Treatment of Metals and Alloys: Techniques and Trends. *Metals*, 2020, vol. 10, no. 9, 1219.
- [12] Petrov P.: Optimization of carbon steel electron-beam hardening. *Journal of Physics Conference Series*, 2010, 223.
- [13] Friedel K.P., Felba J., Wymyslowski A., Pobol I.: A systematic method for optimizing the electron beam hardening process. *Vacuum*, 1996, vol. 47, no. 11, 1317.
- [14] Katsuyuki M., Shiroh U., Takayuki H., Masahiko K.: Electron beam hardening. *International Journal of Materials and Product Technology*, 1990, vol. 5, no. 3.
- [15] Matlák J., Dlouhý I.: Properties of Electron Beam Hardened Layers made by Different Beam Deflection. *Manufacturing Technology*, 2018, vol. 18, no. 2, pp. 279–284.
- [16] Jie Y., Rong W., Deqiang W., Chenggong M., Hui W.: Effect of different scanning modes on the surface properties of continuous electron beam treated 40CrMn steel. *Nuclear Instruments and Methods in Physics Research Section B Beam Interactions with Materials and Atoms*, 2020, vol. 467, pp. 102–107.
- [17] Song R.G., Kepeng Z., Guangliang C.: Electron beam surface treatment. Part I: surface hardening of AISI D3 tool steel. *Vacuum*, 2003, vol. 69, no. 4, pp. 513–516.
- [18] Świątnicki W., Radowski P., Dudzińska K., Wasiak K.: Method for heat treatment of steel. The Patent Office of the Republic of Poland. PAT No. 234490.
- [19] Joshi S., Hildebrand J., Abdulkareem S. Aloraier, Rabczuk T.: Characterization of material properties and heat source parameters in welding simulation of two overlapping beads on a substrate plate. *Computational Materials Science*, 2013, vol. 69, pp. 559–565.
- [20] SYSWORLD 2013 Technical Description of Capabilities.